

Optimization of blazed quantum-grid infrared photodetectors

L. P. Rokhinson,^{a)} C. J. Chen, K. K. Choi,^{b)} and D. C. Tsui
Department of Electrical Engineering, Princeton University, New Jersey 08544

G. A. Vawter
Sandia National Laboratories, Albuquerque, New Mexico 87185

L. Yan, M. Jiang, and T. Tamir
Department of Electrical Engineering, Polytechnic University, Brooklyn, New York 11201

(Received 21 June 1999; accepted for publication 12 October 1999)

In a quantum-grid infrared photodetector (QGIP), the active multiple quantum well material is patterned into a grid structure. The purposes of the grid are, on the one hand, to create additional lateral electron confinement and, on the other, to convert part of the incident light into parallel propagation. With these two unique functions, a QGIP allows intersubband transition to occur in all directions. In this work, we focused on improving the effectiveness of a QGIP in redirecting the propagation of light using a blazed structure. The optimization of the grid parameters in terms of the blaze angle and the periodicity was performed by numerical simulation using the modal transmission-line theory and verified by experiment. With a blazed structure, the sensitivity of a QGIP can be improved by a factor of 1.8 compared with a regular QGIP with rectangular profiles.

© 1999 American Institute of Physics. [S0003-6951(99)02049-5]

Quantum well infrared photodetector (QWIP) technology has matured rapidly in the last several years.¹ The invention of the corrugated light coupling scheme adds to its simplicity, versatility and sensitivity.^{2,3} To further advance the technology, intense efforts have been directed to produce three-dimensional confined structures^{4,5} to overcome the dipole selection rule for optical transition and to increase the carrier lifetime of the detector. Among different approaches, the quantum-grid infrared photodetector (QGIP) structure has been proposed,⁶ in which the additional lateral confinement in a QWIP structure is achieved by patterning the active material into either a lamellar grid or a crossed grid structure. In addition to the expected intrinsic normal incident absorption from the lateral quantization, the grid also serves as a diffraction grating to direct part of the incident light into parallel propagation. With light coming into the detector material from all directions, intersubband transitions in all directions can occur simultaneously, leading to a potentially larger quantum efficiency.

Previously,⁶ we observed that when the line width of the grid is larger than $0.5 \mu\text{m}$, the effects of lateral confinement is negligible, and the grid serves purely as a light diffraction device. For example, the maximum photoresponse of a QGIP occurs when the first-order diffraction angle according to the grating equation is at 90° . At this maximum, the sensitivity of the QGIP was found to be 1.3 times higher than that with the standard 45° edge coupling. This results shows that a QGIP is quite effective in light coupling. In this work, we tried to further improve its coupling efficiency using different grid sidewall profiles. In grating design, it is well known that a blazed reflection grating can shift the optical power from the usual zeroth-order diffraction to the first order by

choosing $2\gamma = \theta$, where γ is the blaze angle and θ is the first-order diffraction angle. According to this prescription, an optimized blaze design for QWIP material would have $\theta = 90^\circ$ (i.e. $p = \lambda/n$) and $\gamma = 45^\circ$, where p is the grid periodicity, λ is the incident wavelength, and n is the average refractive index of the grid. The flexibility of QGIP processing allows arbitrary values of p and γ to be fabricated by directing the reactive ion beam at an oblique angle during material etching.^{7,8} With a proper blazed QGIP (BQGIP) design, a higher coupling efficiency is expected. Figure 1 shows the BQGIPs with both lamellar and crossed grid patterns.

However, it turns out that although the basic concept of a blaze design is useful, the above prescription is not applicable to the present detector geometry. First, the infrared

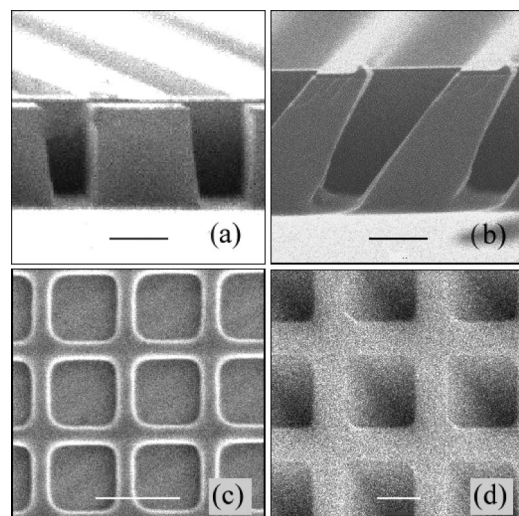


FIG. 1. SEM micrograph of cross section of (a) a rectangular QGIP and (b) a blazed QGIP. A top view of the crossed (c) rectangular and (d) blazed QGIP. All bars are $1 \mu\text{m}$.

^{a)}Electronic mail: leonid@ee.princeton.edu

^{b)}Present address: U.S. Army Research Laboratory, 2800 Power Mill Road, Adelphi, MD 20783.

absorption occurs within the grid material, where optical intensity should be maximized. Second, unlike the usual blazed grating with saw-tooth grooves, each QGIP grid period contains two slanted reflecting surfaces at the side and one parallel reflecting surface at the top. The presence of this internal structure within each period accounts for a collective interference that is more complex than that in saw-tooth profiles. Finally, each grid line contains at the top a metal strip that also affects the electromagnetic (EM) field distribution within the grid. Therefore, rigorous numerical electromagnetic field simulation techniques have to be invoked in this case.

Among different EM field simulation techniques such as the finite-difference time-domain technique,⁹ the beam-propagation method,¹⁰ and various coupled-wave schemes,¹¹ the modal expansion techniques¹² have been very successful in providing both rigorous numerical solutions and important physical insight into problems involving periodic structures. Recently, a modal transmission-line theory¹³ has been developed for multilayered grating structures. In this theory, a general solution of the EM field in every material layer (including the grating region) is expressed in the form of rigorous modal expansions. Each field mode consists of a summation over all the diffracted orders generated by the grating. Appropriate boundary conditions are set up at all interfaces to match each diffraction order across every interface. The problem can then be cast into and solved by an equivalent transmission-line network which provides transfer matrices expressing input-output field relationship in every material layer. In this framework, the EM field distribution generated by the incident infrared radiation is obtained successively from layer to layer by matrix multiplication.

Although the original theory was developed for lamellar dielectric gratings with rectangular profiles, it can be readily extended to those with arbitrary (lamellar) sidewall profiles and to situations involving metal grating strips. For the present detector geometry, we partitioned the blazed grid structure horizontally into a sufficiently large number (twenty or more) of sublayers so that each sublayer can be approximated by a rectangular grating. To include the effects of the metal strips, the total EM field is obtained as the superposition of a primary field and a secondary one. The former is generated by the incident field if the metal strips are absent. The secondary field is due to an equivalent surface current J which is set up at the locations of the metal strips. J is determined by a Galerkin procedure,¹⁴ which satisfies the boundary conditions that (a) the total horizontal electric field at the metal–semiconductor interface is zero and (b) the current J is given by the discontinuity in the horizontal magnetic field across that interface. The details of these procedures will be published by some of the authors in a later publication.¹⁵ Figure 2 shows the numerical result of $|E_x|$ in a typical BQGIP, where E_x is the electric field component vertical to the layers. Intersubband transition of a regular QWIP is known to be directly proportional to $|E_x|^2$.

To assess the effectiveness of a BQGIP in light coupling, we evaluated the ratio α which is the cross-sectional averaged $|E_x|^2$ within the grid material over that of a 45° coupling QWIP, i.e., $\alpha \equiv \langle |E_x|^2 \rangle / \langle |E_x|^2 \rangle_{45}$. We found that for fixed values of γ ($=60^\circ$), line spacing s ($=1.5 \mu\text{m}$), and λ

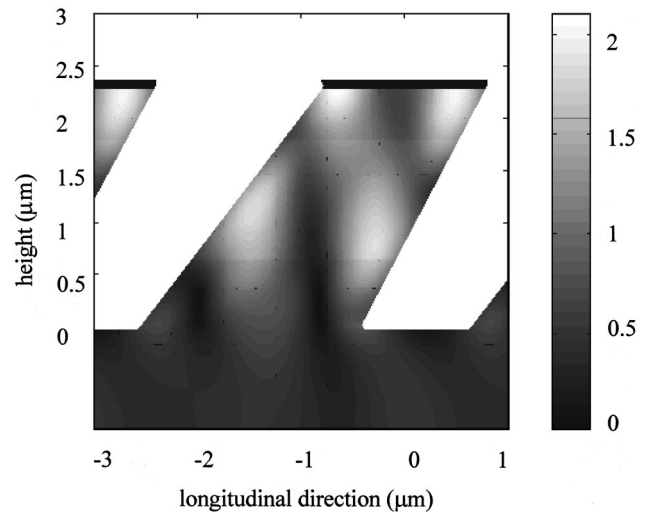


FIG. 2. Distribution of the electric field $|E_x|$, normalized to the magnitude of the incident longitudinal electric field, within a blazed QGIP with $p = 3.2 \mu\text{m}$ and the sidewall profile shown in Fig. 1(b) for $\lambda = 7.6 \mu\text{m}$. Metal is assumed on top of the grid (thick line). The discontinuity of the field lines at the heights 0.65 and 1.8 μm is due to the small change in the dielectric constant between the GaAs contact layers and the AlGaAs/GaAs multiple quantum wells.

($=7.6 \mu\text{m}$), the value of α was peaked at certain values of grid periodicity p when the thickness of the grid line was varied. In the fabricated structures as shown in Fig. 1(b) and Fig. 2, however, the values of γ are slightly different for the two slanted surfaces, being 52° and 62° , respectively. To be more specific, the dashed curve in Fig. 3 shows the theoretical value of α as a function of p for the actual γ experimentally realized. At $p = 3.2 \mu\text{m}$, $\alpha = 2.5$, which means an optimized (lamellar) BQGIP to be 2.5 times more effective than the 45° edge in optical coupling. In order to compare a BQGIP with a regular QGIP with rectangular sidewalls, we

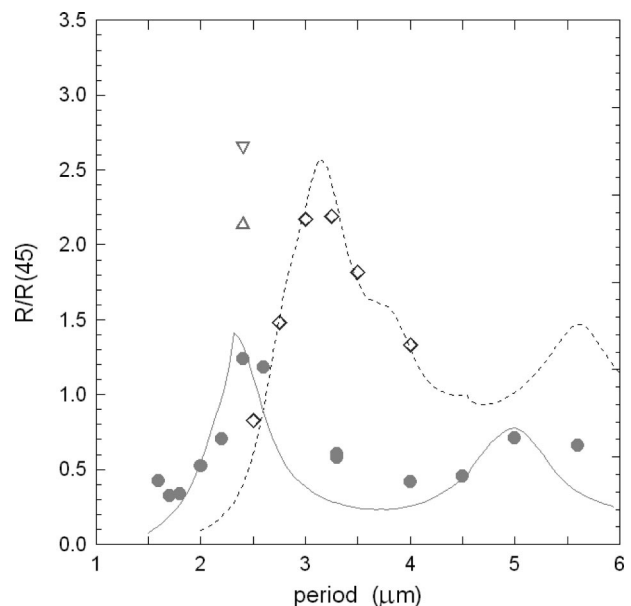


FIG. 3. Measured coupling efficiency $R/R(45)$ of the rectangular QGIPs (\bullet) and the lamellar blazed QGIPs (\diamond) is plotted for samples with different grid periodicity. The solid and dashed curves are the corresponding theoretical curves with no adjustable parameters. (Δ) and (∇) are experimental points for two samples with crossed blazed grid patterns and $w = 0.7$ and $1.0 \mu\text{m}$, respectively.

also calculated α for rectangular QGIPs with $s = 1.0 \mu\text{m}$. The result is shown in Fig. 3 as a solid curve. In this case, α peaks at $p = 2.4 \mu\text{m}$ with a value of 1.4. Hence, the coupling efficiency can be improved at least by 80% from a regular QGIP by adopting a blaze design.

We have fabricated and characterized both the BQGIPs and the regular QGIPs. The QWIP material consists of 20 periods of GaAs/Al_{0.3}Ga_{0.7}As. We have minimized the top contacting area by having a small metal bridge connecting to a separate bonding pad (a detailed description of the sample processing can be found in Ref. 6). Lamellar Ni grid patterns with $146 \mu\text{m} \times 146 \mu\text{m}$ total area were created on the sample surfaces by electron beam lithography and lift-off techniques. The Ni grid serves as a mask in the Cl₂ based reactive-ion-beam etching to remove the unwanted QWIP material. The Ni metal remains on the detector during detector characterization. The etching causes no significant material damage to the sidewalls.⁸ A reference sample with the same total detector area but no patterns was prepared for 45° edge coupling.

In order to determine the coupling efficiency of the grids without the influence from the intrinsic detector properties, the ratio $R/R(45)$ was measured, where R is the photocurrent to dark current ratio of a QGIP and $R(45)$ is that of the reference sample. The photocurrent is measured at 10 K and $\lambda = 7.6 \mu\text{m}$ with a calibrated blackbody source using a lock-in technique. The dark current is the thermally activated current measured at 77 K. By taking the photocurrent to dark current ratio, the detector area, the electron mobility, and the hot-electron escape probability will be cancelled out; R is dependent only on the ratio of the photoelectron density to the thermal electron density. If we further take the ratio $R/R(45)$, the thermal electron density and the effects of the electron doping density and the recombination lifetime on the photoelectron density can also be factored out. The resulting $R/R(45)$ becomes independent of all the intrinsic detector parameters, and it is only a function of the relative optical intensity of the two coupling schemes, i.e., $R/R(45) = \alpha = \langle |E_x|^2 \rangle / \langle |E_x|^2 \rangle_{45}$.

Therefore, the value of $R/R(45)$ can serve as an experimental metric to evaluate a coupling scheme and can be directly compared with the theoretical α without any adjustable parameters. From this discussion, it is clear that the optimization of a coupling scheme and the basic QWIP material structure can be separated from each other. The former amounts to maximizing $R/R(45)$ and the latter amounts to maximizing $R(45)$.

The experimental values of $R/R(45)$ for the rectangular QGIPs (circles) and the BQGIPs (diamonds) are plotted in Fig. 3. The data follow quite accurately the theoretical predictions, especially for the BQGIPs. The maximum of $R/R(45)$ for the BQGIPs was measured to be 77% larger than that of the rectangular QGIPs and 2.3 times better than the 45° edge coupling. This result confirms the effectiveness of a the blazed structure in improving the coupling efficiency. At the same time, the data verify the present modal transmission-line theory quantitatively. The theory predicts accurately both the magnitude of $R/R(45)$ and the location of the peaks in both types of QGIP structures.

In addition to the lamellar BQGIPs, we have also begun to investigate both theoretically and experimentally the BQGIPs with crossed patterns. A crossed blaze grid can be produced by directing the ion beam along one of the diagonal axis of the crossed pattern, with an appropriate oblique angle β relative to the material surface. To yield a value of 60° for γ , β is 50°. In the absence of a more specific theoretical guidance, we have fabricated and characterized two crossed BQGIPs with $p = 2.4 \mu\text{m}$ and linewidth $w = 0.7 \mu\text{m}$ (Δ in Fig. 3) and $1.0 \mu\text{m}$ (∇ in Fig. 3). The data show that $R/R(45)$ is about three times larger than that of a lamellar BQGIP at $p = 2.4 \mu\text{m}$. This difference is larger than the expected factor of two based on the simple assumption that a crossed grid couples to both polarizations of the radiation. Obviously, a three-dimensional extension of the theory is needed to account for the present experimental result and to further optimize the detector. Nevertheless, the coupling efficiency of these unoptimized detectors has already shown 2.7 times larger than that of 45° coupling.

In summary, we have shown that the blazed grid structure offers a new design concept which increases the coupling efficiency of a QGIP. We developed a theory which enables us to calculate and optimize the EM field distribution quantitatively before detector fabrication for the lamellar structures. We have fabricated and characterized the BQGIPs and observed a 77% increase in the coupling efficiency. The experimental result verifies the validity of the present theoretical approach. Further improvement is expected for crossed BQGIPs.

The work was partially supported by the ARO. Sandia is a multiprogram laboratory operated by Sandia Corporation, a Lockheed Martin Company, for the United States Department of Energy under Contract No. DE-AC04-94AL85000.

¹S. D. Gunapala, S. V. Bandara, J. K. Liu, W. Hong, M. Sundaram, P. D. Maker, R. E. Muller, C. A. Shott, and R. Carralejo, IEEE Trans. Electron Devices **ED-45**, 1890 (1998).

²C. J. Chen, K. K. Choi, W. H. Chang, and D. C. Tsui, Appl. Phys. Lett. **71**, 3045 (1997).

³K. K. Choi, C. J. Chen, W. H. Chang, and D. C. Tsui, Proc. SPIE **3379**, 441 (1998).

⁴D. Pan, Y. P. Zeng, M. Y. Kong, J. Wu, Y. Q. Zhu, H. Zhang, J. M. Li, and C. Y. Wang, Electron. Lett. **32**, 1726 (1996).

⁵K. W. Berryman, S. A. Lyon, and A. M. Segev, Appl. Phys. Lett. **70**, 1861 (1998).

⁶L. P. Rokhinson, C. J. Chen, D. C. Tsui, G. A. Vawter, and K. K. Choi, Appl. Phys. Lett. **74**, 759 (1999).

⁷G. A. Vawter, J. F. Klem, and R. E. Leibenguth, J. Vac. Sci. Technol. **12**, 1973 (1994).

⁸R. J. Shul, M. L. Lovejoy, D. L. Hetherington, D. J. Rieger, G. A. Vawter, and J. F. Klem, J. Vac. Sci. Technol. A **12**, 1351 (1994).

⁹W.-P. Huang, C. Xu, S.-T. Chu, and S. K. Chaudhuri, J. Lightwave Technol. **10**, 295 (1992).

¹⁰W.-P. Huang, C. Xu, and B. Little, in *Symposium on Guided-Wave Optoelectronic*, edited by T. Tamir, G. Griffel, and H. L. Bertoni (Plenum, New York, 1995), pp. 423–428.

¹¹M. G. Moharam and T. K. Gaylord, J. Opt. Soc. Am. **71**, 811 (1981).

¹²L. Li, J. Opt. Soc. Am. **10**, 2581 (1993).

¹³T. Tamir and S. Zhang, J. Lightwave Technol. **14**, 914 (1996).

¹⁴T. Itoh, in *Analysis Methods for Electromagnetic Problems*, edited by E. Yamashita (Artech House, Boston, 1990), pp. 380–383.

¹⁵L. Yan, M. Jiang, and T. Tamir (unpublished).